Human Molecular Genetics, 2003, Vol. 12, No. 21 **2863–2871**
DOI: 10.1093/hmg/ddg309

A central nervous system specific mouse model for thanatophoric dysplasia type II

Ti Lin[1], Stacey B. Sandusky[1], Haipeng Xue[2], Kenneth W. Fishbein[3], Richard G. Spencer[3], Mahendra S. Rao[2] and Clair A. Francomano[1,*]

[1]Laboratory of Genetics, National Institute on Aging, Baltimore, Maryland, USA, [2]Laboratory of Neurosciences, National Institute on Aging, Baltimore, Maryland, USA and [3]Laboratory of Clinical Investigation, Nuclear Magnetic Resonance Unit, National Institute on Aging, Baltimore, Maryland, USA

Received July 25, 2003; Revised August 19, 2003; Accepted August 28, 2003

To investigate the specific effect of the Fgfr3 K644E mutation on central nervous system (CNS) development, we have generated tissue-specific TDII mice by crossing *Fgfr3*$^{+/K644E\text{-}neo}$ transgenic mice with CNS-specific Nestin-cre or cartilage-specific Col2a1-cre mice. TDII/Nestin-cre (*TDII-N*) neonates did not demonstrate a profound skeletal phenotype. *TDII-N* pups were comparable to their wild-type littermates in terms of tail length, fore and hindlimbs, and body weight; however, many pups exhibited notably round heads. MRI and histochemical analysis illustrated asymmetric changes in cortical thickness and cerebellar abnormalities in *TDII-N* mice, which correlate with brain abnormalities observed in human TDII patients. Such abnormalities were not seen in TDII/Col2a1-cre (*TDII-C*) mice. Upon examination of adult *TDII-N* spinal cord, premature differentiation of oligodendrocyte progenitors was observed. Overall, these data indicate that the tissue-specific mouse model is an excellent system for studying the role of Fgfr3 in the developing CNS.

INTRODUCTION

Fibroblast growth factor receptors (FGFRs) are encoded by four structurally related genes (FGFR1–4). The receptors display three immunoglobulin-like (Ig) domains, a transmembrane domain, and an intracellular tyrosine kinase domain (1). FGFR3 has an alternative splice site in the third immunoglobulin domain that produces two ligand-specific isoforms. The splice form containing the IIIb isoform is expressed in epithelial cells (2,3), while exon IIIc appears around E10.5, and is detected in the developing mouse brain, spinal cord and all developing long bones (2). *Fgfr3* plays a unique role in the developing nervous system as loss of *Fgfr3* affects both astrocyte and oligodendrocyte differentiation and development (4).

Three distinct mutations in K650 of FGFR3 have attracted considerable attention since each mutation gives rise to a different type of skeletal dysplasia with graded severity. These include hypochondroplasia (HCH : K650N), severe achondroplasia with developmental delay, acanthosis nigricans (SADDAN : K650M) and thanatophoric dysplasia type II (TDII : K650E). Both K650E and K650M result in constitutive activation of FGFR3 tyrosine kinase (5,6).

Thanatophoric dysplasia (TD) is a neonatal lethal skeletal dysplasia, with an estimated frequency of 1 in 35 000 to 1 in 50 000 births (7). TD patients have severely shortened limbs, macrocephaly, short ribs and a hypoplastic thorax. Newborns with TD typically die within the first few days of life (8,9). TD has been divided into two groups. TDI is characterized by the presence of curved femora, less platyspondyly, and usually milder craniosynostosis, whereas TDII is characterized by straight femora and a cloverleaf skull (10). In addition to these abnormalities, a variety of neuropathological findings have been described in the central nervous system (CNS) of TDII patients. Abnormalities of the CNS include bilateral bulging of the temporal lobe, dysplastic hippocampus, cortical polymicrogyria, hypoplastic corpus callosum and pyramidal tracts, and a small brain stem and cerebellum (8,9,11–14).

TDII arises from a single, recurrent mutation (K650E) in the second tyrosine kinase domain of the FGFR3 protein (15). In order to understand how constitutive activation of *Fgfr3* causes TDII, an Fgfr3$^{+/K644E\text{-}neo}$ mouse model was generated with the K644E mutation (corresponding to K650E in humans) (16). This model was designed using the *Cre–loxP* system to control for expression of the K644E mutation.

Until now, the brain pathology of TDII transgenic mice has not been investigated, and the pathogenesis of the CNS phenotype remains unexplained. It is not clear from the clinical phenotype of TDII whether the CNS phenotype is a consequence of

*To whom correspondence should be addressed at: Laboratory of Genetics, National Institute on Aging, 333 Cassell Drive, Baltimore Maryland, 21224-6814, USA. Tel: +1 4105588201; Fax: +1 4105588087; Email: francomanocl@grc.nia.nih.gov

impingement by abnormal skeletal development or the result of a fundamental change in CNS development. To clarify this, we mated *Fgfr3*$^{+/K644E\text{-}neo}$ mice with mice carrying *Cre recombinase* under the control of the nestin promoter (*Nestin-Cre*) so that the K644E is expressed only in the developing CNS and does not affect the skeletal system. The current study demonstrates that the resulting pups, *TDII-N*, exhibit a skeletal phenotype that is comparable to wild-type, and also show severe anatomical malformations in the brain, supporting the hypothesis that CNS manifestations in human TDII patients are caused by direct effects of the Fgfr3 mutation on the developing brain and not because of secondary effects from skull abnormalities.

RESULTS

Generation of tissue-specific TDII mice

A transgenic mouse model was constructed by Iwata *et al.* (16) such that *Fgfr3*$^{+/K644E\text{-}neo}$ mice carried a point mutation in exon 15, A1948G : K644E, as well as a neomycin-resistance gene (*neo*) in intron 10 (Fig. 1A). The A1948G mutation abolished the *Bbs*I restriction site; therefore, *Bbs*I was used to distinguish the mutant allele from the normal allele (Fig. 1B). *Fgfr3*$^{+/K644E\text{-}neo}$ mice hemizygous for the transgenic insert were viable, fertile and normal in size and did not display any gross physical or behavioral abnormalities. When K644E transgenic mice were generated by crossing mice in which the *Cre recombinase* was expressed in all cells (*EIIa-Cre*) with *Fgfr3*$^{+/K644E\text{-}neo}$ mice, the resulting pups, designated *TDII-E*, were much smaller than their wild-type littermates and survived for less than 6 h (Fig. 2A). *TDII-E* pups had a severe skeletal phenotype, reflecting the embryonic onset of the human neonatal lethal dwarfism, TDII. Owing to the brief life span of *TDII-E* pups, ~50% of the pups died before examination of their brains could take place.

Crossing *Nestin-Cre* mice with *Fgfr3*$^{+/K644E\text{-}neo}$ generated CNS-specific TDII transgenic mice (*TDII-N*). *TDII-N* pups displayed a skeletal phenotype comparable to their wild-type littermates (Fig. 2B), yet some pups exhibited a notably round head. Their life span was more than 28 days. We also generated cartilage-specific TDII transgenic mice (*TDII-C*) by crossing *Fgfr3*$^{+/K644E\text{-}neo}$ with *Col2a1-Cre* mice. *TDII-C* pups were smaller than their wild-type littermates (Fig. 2C), and displayed a very severe skeletal phenotype similar to that of *TDII-E*; however, one *TDII-C* pup survived until 20 days after birth. The average body weight of wild-type, *TDII-E*, *TDII-N* and *TDII-C* pups was not significantly different overall ($F_{3,112} = 2.055$, $P = 0.1103$; Fig. 2D). The average tail length of wild-type, *TDII-E*, *TDII-N*, and *TDII-C* pups was significantly different overall ($F_{3,112} = 63.39$, $P < 0.0001$). However, *TDII-N* and wild-type groups were comparable ($P = 0.04$; Fig. 2D).

Brain morphology

Brains of neonatal mice were dissected and subsequently weighed. Brain weight is highly variable within each mouse strain, such that variation within each strain is considerable even after compensating for differences in age, body weight and sex by multiple regression (17). Therefore, we only compared the brain weight within a particular litter. A single newborn *TDII-E* brain was heavier (0.20 g) than that of its single wild-type littermate (0.13 g). In terms of weight, *TDII-N* and *TDII-C* brains were 1.17- and 1.04-fold heavier than their wild-type littermates (Table 1). In both *TDII-E* and *TDII-N* brains, the cerebral cortex was enlarged and pushed outward laterally (Fig. 3A and B). The abnormal brain pathology was even more obvious in 28-day-old *TDII-N* pups ($n = 3$; Fig. 3C), where the weight of the *TDII-N* brain was 1.35 times that of the wild-type brain. In terms of brain size, the P28 *TDII-N* brain was expanded both laterally and longitudinally compared with the wild-type littermate (Fig. 3C).

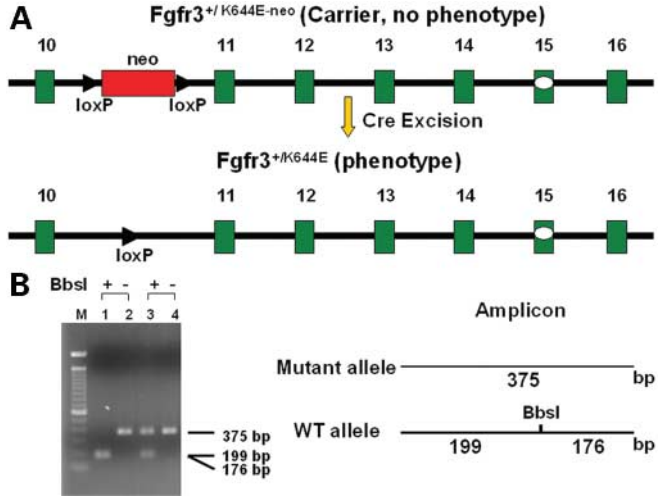

Figure 1. Generation and identification of Fgfr3 transgenic mice. (**A**) *Fgfr3*$^{+/K644E\text{-}neo}$ mice were created using a 'knock-in' strategy. The *Cre–loxP* recombination system was employed to excise the *neo* gene in later generations. The mutation was co-transferred with the *neo* gene, which was flanked by two *loxP* sites, through homologous recombination. Transgenic mice carrying the K644E mutation along with *neo* were phenotypically normal due to the suppression of mutations by *neo.* When transgenic mice mated with tissue-specific cre mice carrying the *Cre recombinase* gene under the control of different tissue-specific promoters, the *neo* gene was excised and the mutation was expressed in a tissue-specific manner. (**B**) Fgfr3 amplicon containing exon 15 was digested with *BbsI* to confirm presence of the K644E mutation. The *Bbs*I restriction site was abolished due to the K644E mutation; therefore we used a *Bbs*I digest to distinguish the mutant from the wild-type allele. The size of the mutant amplicon was 375 bp, whereas the wild-type amplicon consisted of two bands located at 199 and 176 bp after digestion. Lane M, 100 bp marker; lanes 1–2, wild-type DNA; lane 3–4, heterozygous DNA.

Efficiency of Cre recombinase

In order to verify the efficiency of Cre activity in the brains of TDII pups, a male *Nestin-Cre* was mated with the reporter mouse strain *Bgeo/GFP* (female). *Cre recombinase* activity is driven by the nestin promoter, such that nestin immunoreactive cells should have Cre activity and express GFP. Any cells expressing nestin at any time in development should be GFP-positive. GFP expression was detected using a microscope without antibody, and was detected in ~10% of neurons in both the brain (Fig. 4A and B) and spinal cord (Fig. 4C and D) of newborn *TDII-N* pups. This result is consistent with the

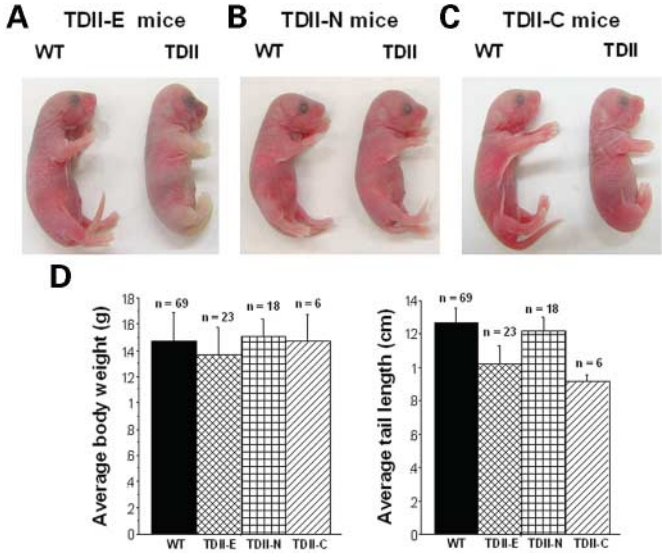

Figure 2. Skeletal morphology and physical attributes of tissue-specific TDII pups. *TDII-E* pups displayed the most severe skeletal phenotype (**A**), with shortened fore and hindlimbs, a shortened tail, and a notably round head compared with their wild-type littermates. They consistently lived less than 6 h. *TDII-N* pups (**B**) exhibited no obvious skeletal deformities and were comparable to their wild-type littermates in terms of fore and hindlimbs, and tail length. They also showed a notably round head, although this feature was not as prominent as in the *TDII-E* pups. Their lifespan was 7–28 days. All pups still alive at 28 days were euthanized. *TDII-C* pups also had a severe skeletal phenotype (**C**) with stubby fore and hindlimbs, and a shortened tail. A single pup lived 20 days after birth. (**D**) Average body weight and tail length of wild-type and TDII pups was calculated. The difference among group sample means (for body weight and tail length) was calculated with an ANOVA. No significant differences were observed between wild-type and TDII groups for average body weight, however significant differences between wild-type and *TDII-E*, and *TDII-E* and *TDII-N* were observed for average tail length. A *P*-value of < 0.0083 was considered significant. Error bars represent standard deviations from the means.

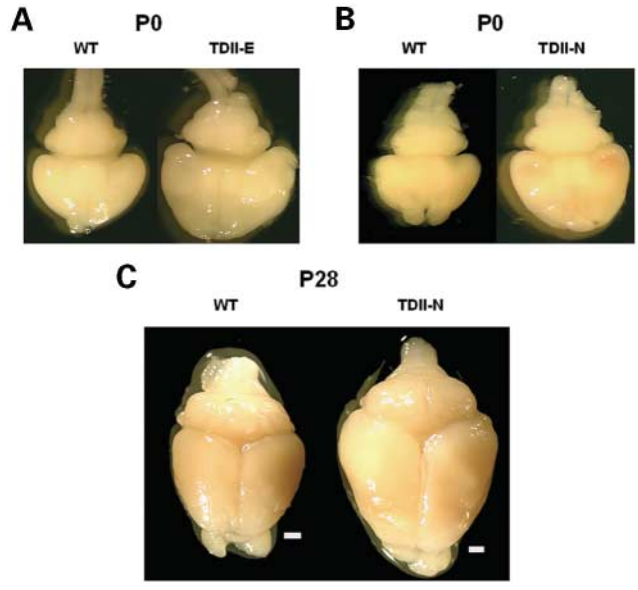

Figure 3. Brain morphology of TDII pups. (**A**) Brain of a P0 *TDII-E* pup (right) and its wild-type littermate (left). *TDII-E* pups had grossly enlarged brains, with a considerable increase in the surface area of the cerebral cortex. (**B**) Brain of a *TDII-N* pup and its wild-type littermate. *TDII-N* pups also had an enlarged cerebral cortex. (**C**) The brain of *TDII-N* at day 28 had an even more prominent cerebral cortex compared to its wild-type littermate. Scale bar, 1000 μm.

Table 1. P0 average brain weight (g)

	TDII-E (*n*)	TDII-N (*n*)	TDII-C (*n*)
WT	0.130 (1)	0.144 ± 0.018 (5)	0.108 ± 0.023 (4)
TDII	0.200 (1)	0.169 ± 0.023 (3)	0.113 (1)

observation on *Cre recombinase* efficiency in brain conducted by Metzger and Chambon (18).

MRI of TDII brains

Newborn wild-type and TDII brains were analyzed by MRI. Compared with wild-type (Fig. 5A), the brains of *TDII-E* (Fig. 5B) and *TDII-N* (Fig. 5C) pups were asymmetric and misshapen, and both had enlarged lateral ventricles. *TDII-C* did not appear to have any obvious brain deformation, and was comparable to wild-type (Fig. 5D). The average brain volume of wild-type, *TDII-E*, *TDII-N*, and *TDII-C* mice was significantly different overall ($F_{3,13} = 10.781$, $P = 0.0008$) (Fig. 5E). In pairwise comparisons, the average brain volume was significantly different between wild-type and *TDII-E* ($P = 0.0016$), wild-type and *TDII-N* ($P < 0.0004$), and *TDII-N* and *TDII-C* ($P = 0.0041$). There was no significant difference in average brain volume between wild type and *TDII-C*, *TDII-E* and *TDII-N*, or *TDII-E* and *TDII-C* mice. The average brain width and length of wild-type, *TDII-E*, *TDII-N* and *TDII-C* mice was significantly different overall (width, $F_{3,13} = 15.834$, $P = 0.0001$; length, $F_{3,13} = 9.738$, $P < 0.0012$). The average brain height of all four groups was not significantly different ($F_{3,13} = 2.922$, $P = 0.074$; Fig. 5F). In pairwise comparisons of average brain width, there were significant differences between wild-type and *TDII-E* ($P = 0.0081$), wild-type and *TDII-N* ($P < 0.0001$), *TDII-E* and *TDII-C* ($P = 0.0021$), and *TDII-N* and *TDII-C* ($P < 0.0001$) mice. The average brain length was also significantly different between wild-type and *TDII-N* ($P = 0.0003$), *TDII-E* and *TDII-N* ($P = 0.0006$), and *TDII-N* and *TDII-C* mice ($P = 0.0013$).

Histology and immunohistochemistry findings

Both *TDII-E* (Fig. 6B) and *TDII-N* (Fig. 6C) brain sections showed asymmetry of the forebrain hemisphere compared with wild-type pups (Fig. 6A). Lateral and third ventricles were enlarged, deformed and misplaced (Fig. 6B and C). There was gross disorganization of the hippocampus and considerable disorientation of the pyramidal cells in both coronal sections compared to wild-type mice (Fig. 6B and C). The pia layer from *TDII-E* and *N* cortices (Fig. 6E and F) was discernable from wild-type (Fig. 6D) by its uneven surface. Higher magnification of coronal sections illustrated an increased number of heterotopic neurons accumulated in the cortical plate zone (Fig. 6E and F). The marginal zone did not appear to differ in size or cell type between transgenic and wild-type. Overall, layer boundaries in cortices were blurred and indistinct

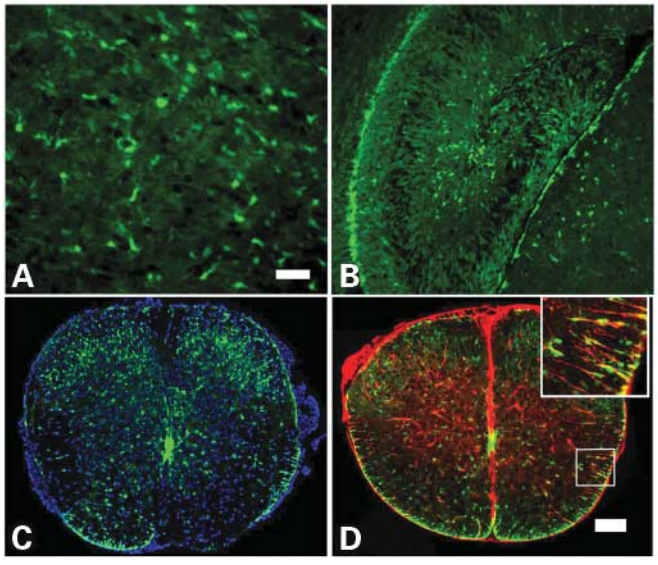

Figure 4. Efficiency of Cre recombinase. Brain and spinal cord sections were collected from P0 pups generated from mating *Nestin-Cre* with *Bgeo/GFP*. Fixed sections were processed for immunohistochemistry to examine the expression of GFP (green, **A**–**D**) and nestin (red, D). Sections were counterstained with DAPI to localize all nuclei (blue, C). Approximately 10% of the cells were GFP positive in the thalamus (A) and hippocampus. (B). In P0 spinal cord, more than 10% of the cells were GFP positive. (C) More GFP immunoreactive cells were observed in the dorsal domain of the spinal cord than in the ventral. (D) Double labeling of nestin (red, D) and GFP (green, D) showed that only a small percentage of nestin immunoreactive cells coexpress GFP. Scale bar, 10 μm for (A) and 100 μm for (B), (C) and (D).

in mutant brains. Sagittal sections of the hippocampus showed accumulation of aberrant neurons in the dentate gyrus and CA1 (Fig. 6H and I). The fourth ventricle of both transgenic brains (Fig. 6K and L) was hypoplastic compared with the wild-type (Fig. 6J). Misshapen lobes of the cerebellum and decreased epithelial cells of the choroid plexus were observed in *TDII-E* and *N*, respectively (Fig. 6K and L).

Since abnormalities were seen throughout the rostrocaudal axis and were present early in development, we examined whether abnormalities were specific to a particular class of cells. Coronal spinal cord sections from newborn wild-type and *TDII-N* pups were prepared and markers of astrocyte, oligodendrocyte and neuronal development were examined. In P0, early markers of stem cells and precursors such as Sox1 and Olig2 were distributed normally (data not shown). No difference in expression of astrocyte marker GFAP in P0 spinal cord was observed between wild-type and *TDII-N* (Fig. 7A and B). Similarly, βIII tubulin showed no difference in expression (Fig. 7C and D). However, increased expression of oligodendrocyte marker GalC was observed in the ventral area of P0 *TDII-N* spinal cord (Fig. 7F). At P24, enhanced expression of GFAP was observed in the gray matter of *TDII-N* spinal cord compared to its wild-type littermate (Fig. 8A and B). Premature expression of GalC in *TDII-N* (Fig. 8F) was also observed. The initial pattern of neuronal differentiation was normal in all *TDII-N* spinal cords at P0 by staining with neuron specific marker βIII tubulin. Extensive neuronal loss was seen (Fig. 8C and D) after a small litter of pups ($n = 2$) was sacrificed at P24. Since proliferation results did not show any alterations in Ki-67 expression (Fig. 9A and B) or BrdU incorporation (Fig. 9C and D), these data suggest that a secondary neuronal loss is due to a primary defect in oligodendrocyte and astrocyte differentiation. These results are consistent with data showing a delay in myelination in Fgfr3 null mice and primary localization of *Fgfr3* expression to glial cells (4).

DISCUSSION

Tissue-specific TDII transgenic mouse models were generated by crossing the carrier ($Fgfr3^{+/K644E\text{-}neo}$) with *Nestin-Cre* and *Col2a1-Cre* mice. *TDII-N* mice had brain abnormalities similar to those observed in human TDII patients. The pathogenesis of dysgenetic changes, which are predominantly located in the temporal lobe and lateral ventricles in human TDII, remains unclear. In this study, we focused on whether the CNS phenotype was a consequence of impingement by abnormal skeletal development or the result of a fundamental effect on CNS development. Several reports have discussed this issue. One report suggested that the temporal bulging was not caused by hydrocephalus, but was associated with chondrodystrophy (13). Another report (19) speculated that the agenesis of the corpus callosum and cloverleaf skull were due to developmental rather than deformational factors operating early in maturation. Using the *Nestin-Cre* tissue-specific model, we generated mice that exhibited the following features: dilated lateral ventricles, an enlarged cerebral cortex and disorganized hippocampi. These brain abnormalities support the theory that the abnormal brain in TDII is caused by a developmental brain malformation rather than brain deformation by the skeleton.

The cause of death in neonatal TDII mice also remains to be elucidated. *TDII-N* pups were able to live more than 4 weeks while *TDII-E* pups died within the first 6 h of birth, suggesting that the short lifespan observed in human TDII patients is not the consequence of brain malformation alone. Our *TDII-C* pups displayed a severe skeletal phenotype and lived no more than 20 days. These data suggest that abnormal brain pathology is not the direct cause of death in TDII mice but may contribute to neonatal mortality.

The efficiency of excision mediated by *Cre-loxP* is known to differ in different tissues (18). Our results indicated that the reporter gene GFP was detected in ∼10% of neurons, which is consistent with observations on *Cre recombinase* efficiency in an experiment conducted by Metzger and Chambon (18). GFP is an indirect measure of *Nestin-Cre* recombinase activity, and we are currently working on direct detection of *Fgfr3* K644E expression in *TDII-N* brain. Despite the apparently low excision efficiency of *neo* in TDII transgenic pups, a severe phenotype in the brain was nonetheless observed in our system. A possible explanation for this seeming paradox is that Fgfr3 acts as a homodimer, and is able to form dimers with other FGFR monomers such as FGFR1 (20). The promiscuous dimerization effect may contribute to the severity of the observed phenotype.

In mice, *Fgfr3* is expressed throughout embryonic development (E9.5–E14.5) and into the early stages of fetal growth (E14.5–E16.5). *Fgfr3* is also expressed in the ventricular zone of the developing spinal cord and in glia-like cells in P0 and the

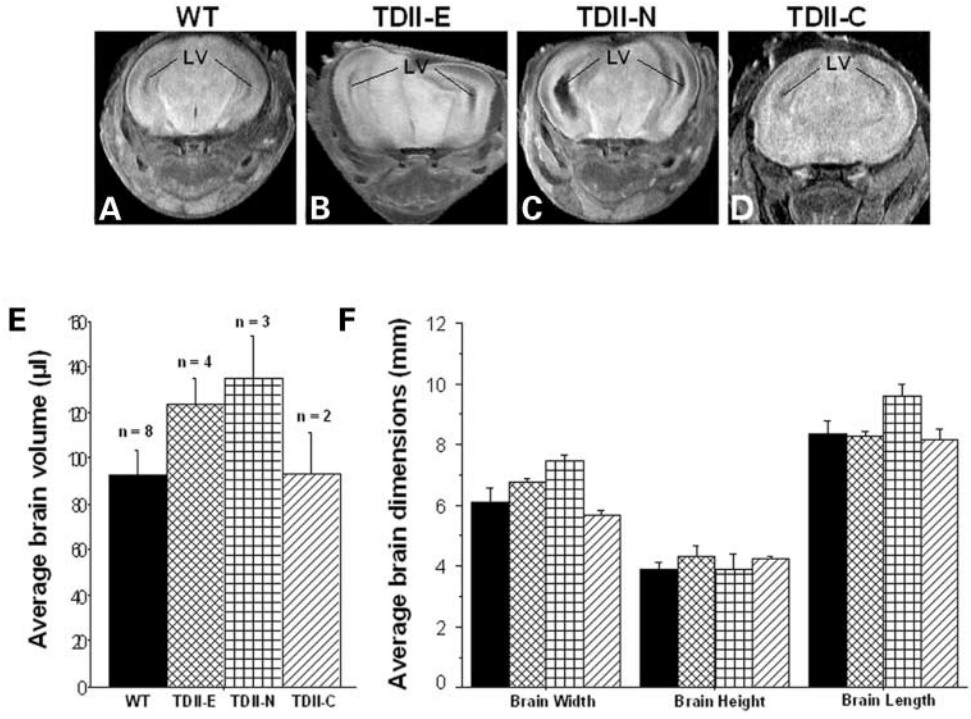

Figure 5. MRI analysis of P0 brains. Panels are coronal brain sections. No brain abnormalities were observed in wild-type mice (**A**). In contrast, *TDII-E* (**B**) and *TDII-N* (**C**) showed brain asymmetry and enlargement of lateral ventricles. *TDII-C* pups (**D**) had a normal cerebral cortex and lateral ventricles. LV, lateral ventricles. (**E**) Overall significant differences were observed in average brain volume between wild-type and *TDII-E*, *TDII-N* and *TDII-C* ($F_{3,13} = 10.781$, $P < 0.0008$). (**F**) Average brain width and length between wild-type, *TDII-E*, *TDII-N* and *TDII-C* were significantly different overall ($F_{3,13} = 15.834$, $P < 0.0001$ for width; $F_{3,13} = 9.738$, $P < 0.0001$ for length). The average brain height between all four groups was not significantly different (number of pups in each group: wild-type = 8, *TDII-E* = 4, *TDII-N* = 3, *TDII-C* = 2).

adult mouse brain (21). A recent report found that *Fgfr3* expression is detected in the nuclei of the choroid plexus at E12.5, E15.5 and E18.5 of the developing mouse brain (22). In rat CNS culture cells, *Fgfr3* is expressed in late oligodendrocyte progenitors and also highly expressed in astrocytes (23). *In vivo*, *Fgfr3* expression was reported in neuroepithelial (NEP) cells and astrocytes in early stages of development (24) and its temporal pattern of expression has suggested that it may identify glial progenitors and regulate their maturation or differentiation.

Our data showed that overgrowth and undergrowth coexist in *TDII-N* newborn brains as has been described in human TDII (9). Evidently, *Fgfr3* participates in cell proliferation, differentiation and even ventricle formation and CSF secretion during brain development. The underlying mechanism whereby the activated *Fgfr3* K644E regulates neuron cells during CNS development remains unclear. Our analysis of *TDII-N* mice suggested that neural abnormalities observed were due to defects intrinsic to the nervous system. Fgfr3 null mice had increased GFAP expression in the spinal cord, cerebellum, and hindbrain compared with wild-type (4). In addition, Fgfr3 null mice demonstrate reduced numbers of differentiated oligodendrocytes in the forebrain, hindbrain, cerebellum and spinal cord with a delay in myelination (4). Present results that show alterations in glial development are consistent with these observations. Our results suggest that constitutive activation of Fgfr3 leads to enhanced, premature differentiation of GalC immunoreactive oligodendrocyte progenitors.

BrdU incorporation showed no difference in cell proliferation between P0 wild-type and *TDII-N* spinal cord. This suggests that other factors have reduced neuronal number in the spinal cord. In addition to the effect on oligodendrocytes, we also noted an increase in astrocyte number and a reduction in neurons. The effect on neuronal number was probably secondary to the changes in glial cells as initial distribution of βIII tubulin expression and number of immunoreactive cells appeared normal at a time when the difference in oligodendrocyte maturation was already apparent. Dramatic reduction in neuronal number, however, could be readily discerned by P24, suggesting a late degeneration.

In summary, these studies demonstrate that brain abnormalities observed in TDII are the result of developmental effects of Fgfr3 constitutive activation on the brain, and not the result of skeletal deformation. The CNS abnormalities are consistent with alterations in glial proliferation and differentiation with a late secondary effect on neuronal survival. Future experiments will examine the stage specific effects of constitutive Fgfr3 activation in individual cell lineages.

MATERIALS AND METHODS

Animal experimentation

All experiments involving use of animals were approved by the Institutional Animal Care and Use Committees (IACUC) at the

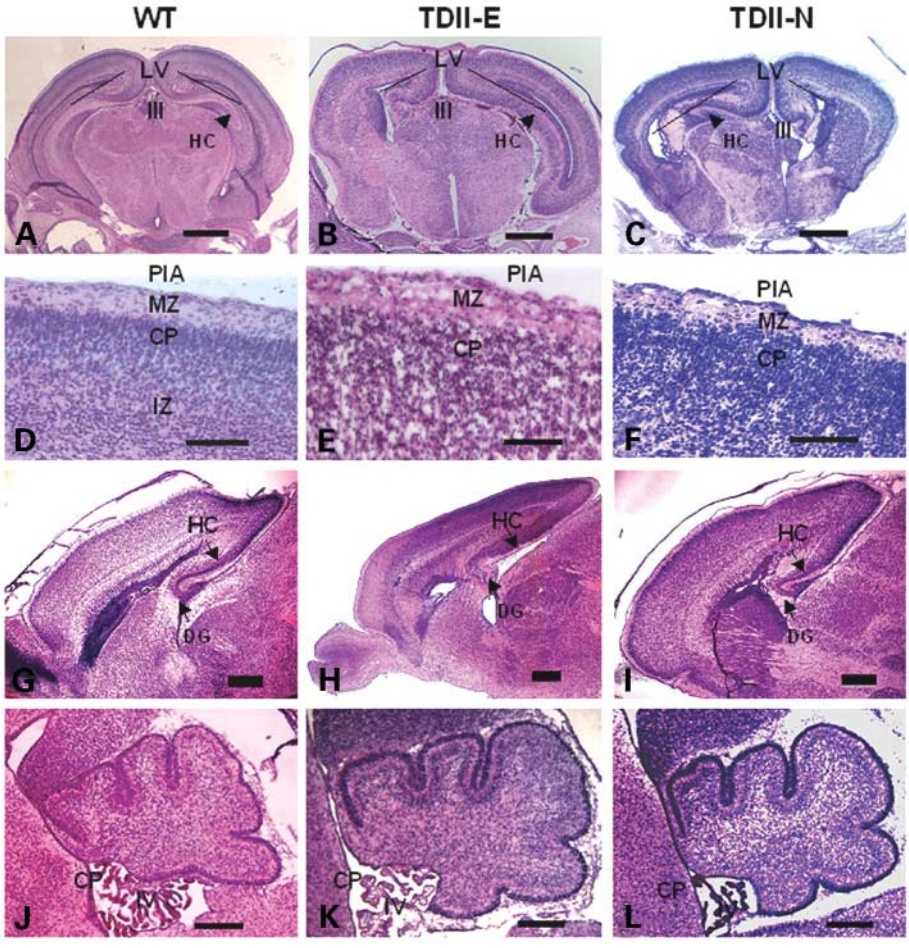

Figure 6. Histochemical analysis of P0 brains. Histoanatomy of whole brain, cortical layers, hippocampus, and cerebellum in wild-type and mutant mice. Coronal brain sections are observed in (A)–(F). Brain hemispheres of the wild-type section (**A**) were symmetric, with no dilation of the lateral ventricles. *TDII-E* (**B**) and *TDII-N* (**C**) both had misshapen, enlarged lateral and third ventricles. Hippocampi of *TDII-E* and *TDII-N* were also both disorganized. Scale bar, 1000 µm. Cortices can be seen in (**D**)–(**F**). The pia from both *TDII-E* (E) and *N* (F) was considerably rough. In *TDII-E* (E) and *N* (F) mice, the cortical plate was thickened with disorganized clusters of cells. Accumulation of ectopic neurons in the cotical plate resulted in indistinct cortices. Scale bar, 40 µm. (**G**)–(**I**) Sagittal sections of the brain. In *TDII-E* mice (H), ectopic neurons in the ventricular zone were compacted, which led to compression of the corpus callosum. The hippocampus was grossly disorganized. Part of the cerebral cortex was thicker in *TDII-N* (I), with ectopic neurons banking in the dentate gyrus. The olfactory bulb in *TDII-N* was missing due to technical difficulties in removing the brain from the skull. Scale bar, 100 µm. Sagittal sections of the cerebellum are in (**J**)-(**L**). In *TDII-E* (K) and *TDII-N* (L) mice, there was simplification of the lobular structure of the cerebellum. The epithelial cells of the choroid plexus were also reduced. Scale bar, 200 µm. LV, lateral ventricles; III, third ventricle; PIA, pia layer; MZ, marginal zone; CP, cortical plate; IZ, intermediate zone; HC, hippocampus; DG, dentate gyrus; CP, choroid plexus; IV, fourth ventricle.

NIA. Animals were maintained in an approved animal facility until required for the experiments. Animals were sacrificed by CO_2 inhalation as recommended by the IACUC.

Mouse strains and breeding

Fgfr3$^{+/K644E\text{-}neo}$ mice were maintained by mating with wild-type. Briefly, an A to G substitution at nucleotide 1948 of the Fgfr3 gene was made by using site directed mutagenesis, and a *neo* flanked by two *loxP* sites was inserted in intron 10 (16). Mice carrying the K644E mutation along with the *neo* gene have a normal life span and are fertile. These mice were used as breeders, thus they serve as 'carriers'. Excision of the *neo* gene was accomplished by mating *Fgfr3*$^{+/K644E\text{-}neo}$ with cre mice carrying the *Cre recombinase* gene under the control of three different promoters. Mouse strains *Ella-Cre*, *Nestin-Cre*, and *Col2a1-Cre* were obtained from Jackson Laboratory (Bar Harbor, ME, USA) and mated with *Fgfr3*$^{+/K644E\text{-}neo}$ to generate TDII transgenic mice (*TDII/Ella-Cre*, *TDII-E*, *TDII/Nestin-Cre*, *TDII-N*; and *TDII/Col2a1-Cre*, *TDII-C*). *Bgeo/GFP* was also purchased from Jackson Laboratory for *Cre recombinase* efficiency testing. The nomenclature of transgenic mice can be found in Table 2. Animals produced from these matings were collected on the first day of birth (P0), and subsequently sacrificed for collection of tissues.

Genotype analysis

To confirm genotypes of *Fgfr3*$^{+/K644E\text{-}neo}$ mice, PCR was performed using primers F1676 (5′-GGGTGATCGTTTGC-CTGAGC-3′) and R2080 (5′-TTCAGATCTCCCTACCCC-CAT-3′). Amplification was with 30 cycles of 94°C for 30 s,

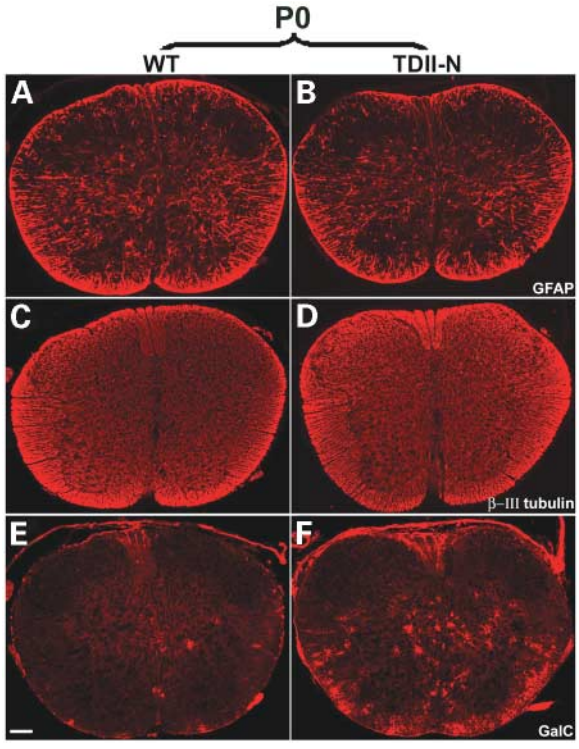

Figure 7. Increased expression of oligodendrocyte marker GalC was detected in P0 *TDII-N* pups. Spinal cord sections from P0 *TDII-N* pups and wild-type littermates were processed to examine the expression of astrocyte marker GFAP (**A**, **B**), neuronal marker β-III tubulin (**C**, **D**), and oligodendrocyte marker GalC (**E**, **F**). Three sections from both wild-type and *TDII-N* were analyzed, and then repeated in a second mouse. Representative sections are shown. No apparent change in the expression of GFAP or β-III tubulin was found in wild-type (A, C) or *TDII-N* neonates (B, D), while more GalC immunoreactive cells were present in the mutant gray and white matter (F). Scale bar, 100 μm.

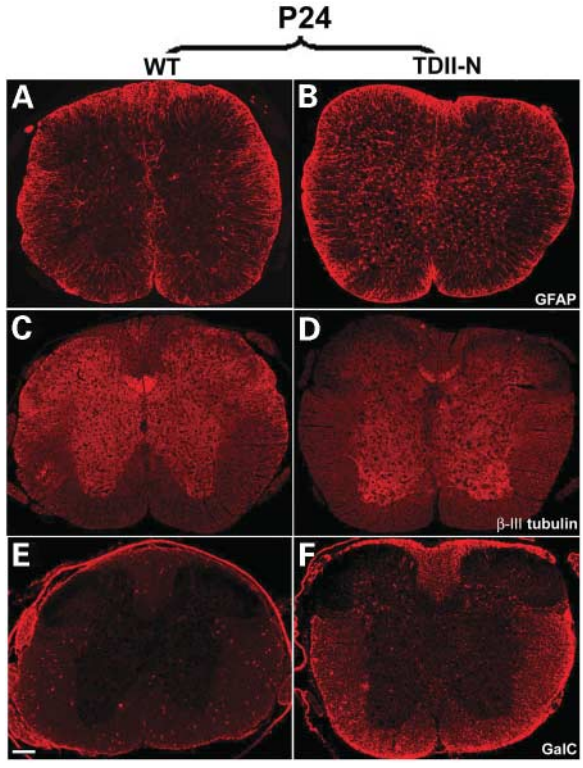

Figure 8. Expression patterns of neuronal, oligodendrocyte and astrocyte markers were altered in P24 *TDII-N* mice. Spinal cord sections from P24 *TDII-N* mice and wild-type littermates were processed to examine expression of astrocyte marker GFAP (**A**, **B**), neuronal marker β-III tubulin (**C**, **D**), and oligodendrocyte marker GalC (**E**, **F**). Three sections from wild-type and *TDII-N* were analyzed. Representative sections are shown. Compared with wild-type (A), more GFAP immunoreactive cells were found in *TDII-N* mice, and the positive cells had shorter fibers with extensive branching for cells located in the gray matter (B). In the mutant spinal cord sections, expression of β-III tubulin was absent in the dorsal funiculus, and more β-III tubulin positive cells were located in the ventral horn (D). Compared with the sporadic staining pattern of GalC in the wild-type (E), the mutant spinal cord showed an increased number of GalC immunoreactive cells in the ventral white matter (F). Scale bar, 100 μm.

55°C for 30 s, and 72°C for 1 min. Following PCR, products were digested with *Bbs*I. Genotypes were determined by PCR of tail DNA from *TDII-N* mice, using primers Nes-F1 (5′-GCGGTCTGGCAGTAAAAACTATC-3′) and Nes-R1 (5′-GTCAAACAGCATTGCTGTCACTT-3′).

Cycling conditions were: 40 cycles of 94°C for 20 s, 58°C for 30 s, 72°C for 35 s, with the first 10 touchdown cycles. *TDII-C* mice were genotyped with primers ColCre-F1 (5′-ACCAGCCAGCTATCAACTCG-3′) and ColCre-R1 (5′-TTACATTGGTCCA-GCCACC-3′). Cycling conditions were the same as *TDII-N*. Since *TDII-E* mice are homozygous for *Cre recombinase*, genotyping was not necessary.

Table 2. Glossary of Fgfr3 transgenic mice

Mouse strains	Characteristics	Phenotype
$Fgfr3^{+/K644E\text{-}neo}$	Carrier, full lifespan	Normal
TDII-E	K644E mutation expressed in all tissues, live less than 6 h	Severe skeletal phenotype
TDII-N	K644E mutation expressed in CNS, live more than 28 days	Mild skeletal phenotype
TDII-C	K644E mutation expressed in cartilage, maximum lifespan is 20 days	Severe skeletal phenotype

MRI

Intact P0 transgenic mice were thawed after being stored at −20°C, and placed on a specially designed stage and inserted into a Bruker DMX 400 NMR spectrometer (Bruker Medizintechnik, Ettlingen, Germany) equipped with a Magnex 9.4 T superwidebore magnet (Magnex Scientific, Abingdon, UK) and a Bruker Micro2.5 microimaging probe. Cold air, supplied by a vortex tube (Exair, Cincinnati, OH, USA), was blown through the probe to refrigerate the neonate. The temperature of the refrigerating air was regulated at 4.0 ± 0.1°C. A series of pilot scans was acquired in order to define axial, sagittal and coronal slices through the body and brain. Diffusion-weighted two-dimensional spin echo MRI images were acquired with specific slice schemes using a diffusion gradient strength of 250 mT/m, duration (δ) of 5 ms and separation (Δ) of 11.5 ms. All images were acquired with repetition time $TR = 5$ s and echo time $TE = 23.2$ ms. Typically, images were acquired with a matrix size of 512×256 pixels,

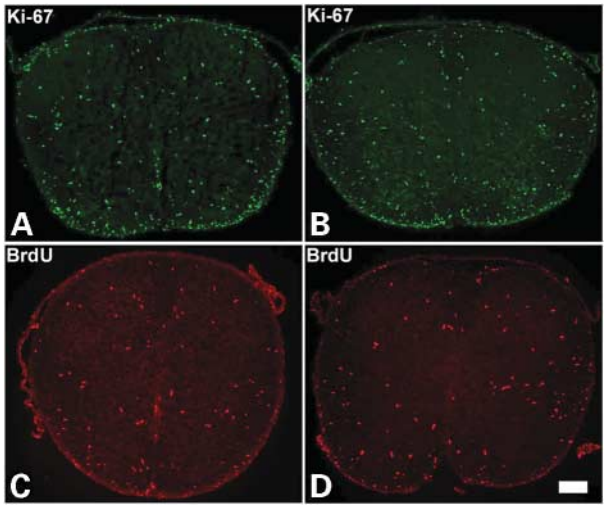

Figure 9. Proliferation analysis of P0 pup spinal cord. There were no differences in Ki-67 staining between *TDII-N* (left) and wild-type (right) spinal cords (**A**, **B**). There were also no differences in BrdU staining between *TDII-N* (left) and wild-type (**C**, **D**). Scale bar, 100 μm.

field of view 2×2 cm or 4×2 cm and slice thickness 0.5 mm, resulting in volumetric resolution of $39 \times 78 \times 500$ μm or $78 \times 78 \times 500$ μm. For each slice scheme (axial, coronal or sagittal; brain or body-centered), scanning time was either 1 h 25 min (with four averages) or 2 h 50 min (with eight averages).

MRI images were processed using Bruker ParaVision software. From the two-dimensional diffusion-weighted images, slices were selected with matching anatomical landmarks for each pup and were scaled uniformly for visual comparison. Brain volumes were calculated by manually tracing the exterior edges of brain tissue in contiguous axial slices, summing the brain area in each slice, and multiplying by the slice thickness (500 μm). Typically, 30–40 slices were analyzed, spanning the entire rostral–caudal length of the brain. Sagittal slices of the brain were selected to coincide with the brain midline for comparison between mice. Overall brain height was calculated by measuring the axial slice with the longest distance from the base of the brain to the inside of the skull. Similarly, the maximum width of the brain was calculated by measuring the axial slice where the brain was widest. The total length of the brain was calculated by measuring the midline sagittal slice, where the length was the distance from the tip of the olfactory lobe to the bend where the brain stem meets the spinal cord.

Histology and immunohistochemistry

Brains and spinal cords were dissected from P0 transgenic and wild-type mice, and fixed and sectioned as previously described (25). P0 tissues were fixed in 4% paraformaldehyde (PFA) for 2 h at 4°C and washed three times with PBS. P24 tissues were fixed overnight. Samples were then cryopreserved with a 10–30% sucrose gradient and embedded in optimal cutting temperature compound (OCT). OCT embedded frozen tissues (12 μm) were sectioned in a sagittal, coronal or transverse manner, and collected on SuperFrost Plus microscope slides (Fisher Scientific, Pittsburgh, PA, USA). Sections were stained with hematoxylin and eosin (H&E) and then imaged with an Axiovert 200 microscope.

For immunohistochemical analysis, sections were blocked in blocking buffer (5% goat serum, 1% bovine serum albumin, 0.1% Triton X-100) for 1 h prior to the application of the primary antibodies, which were incubated overnight at 4°C. A 3 min wash followed, and then the secondary antibody was applied for 30 min at room temperature. The following primary antibodies were used: βIII tubulin (1 : 500; Sigma-Aldrich, St Louis, MO, USA), galactocerebroside (GalC; 1 : 5; a kind gift from Dr Barbara Ranscht), Nestin (1 : 5; DSHB, Iowa City, IA, USA), and glial fibrillary acidic protein (GFAP; 1 : 500; Dako, Carpinteria, CA, USA). The following secondary antibodies were used: TRITC-conjugated anti-mouse IgG2b (1 : 200; Southern Biotechnology, Birmingham, AL, USA), anti-mouse IgG 568 (1 : 500; Molecular Probes, Eugene, OR, USA), and anti-rabbit IgG 568 (1 : 500; Molecular Probes, Eugene, OR, USA).

Cell proliferation detection

Pregnant dams were given a single, intraperitoneal injection of the thymidine analog, BrdU (Sigma-Aldrich, St Louis, MO, USA) at a concentration of 100 μg/mg of body weight for 14 h. P0 pups were perfused and processed as described above. BrdU was detected in sections as described previously (23).

Serial 12 μm sections were air-dried and fixed in 4% PFA for Ki-67 immunostaining. Sections were placed in 10 mM citrate buffer (pre-warmed to 95°C) for at least 15 min and then blocked in blocking buffer (5% goat serum, 1% bovine serum albumin, 0.1% Triton X-100) for 1 h. Sections were incubated with anti-Ki-67 antibody (1 : 25; Dako, Carpinteria, CA, USA) for 30 min to 2 h at room temperature, and were then rinsed with PBS for 5 min three times and incubated with secondary antibody (anti-rabbit IgG 568, 1 : 500; Molecular Probes, Eugene, OR, USA) for 15 min at room temperature. After three 5 min washes with PBS, sections were imaged.

Statistical analysis

Statistical analyses were performed using StatView 5.0.1 (SAS Institute, Cary, NC, USA). The difference among group sample means (for body weight, tail length, brain volume, and brain dimensions) was calculated with a one-way ANOVA. When a significant main effect was observed, Bonferroni–Dunn *post hoc* comparisons were conducted to determine differences between groups. To avoid making a type I error on any one comparison, statistical significance was assessed at a level of $P < 0.0083$, obtained by dividing 0.05 by the number of comparisons.

ACKNOWLEDGEMENTS

We gratefully acknowledge the input from all members of our laboratory provided through discussion and constructive criticism. The nestin antibody was obtained from the Developmental Studies Hybridoma Bank (DSHB) developed

under the auspices of the NICHD and maintained by The University of Iowa.

REFERENCES

1. Schlessinger, J. (2000) Cell signaling by receptor tyrosine kinases. *Cell*, **103**, 211–225.
2. Wuechner, C., Nordqvist, A.C., Winterpacht, A., Zabel, B. and Schalling, M. (1996) Developmental expression of splicing variants of fibroblast growth factor receptor 3 (FGFR3) in mouse. *Int. J. Dev. Biol.*, **40**, 1185–1188.
3. Kanai, M., Rosenberg, I. and Podolsky, D.K. (1997) Cytokine regulation of fibroblast growth factor receptor 3 IIIb in intestinal epithelial cells. *Am. J. Physiol.*, **272**, G885–G893.
4. Oh, L.Y., Denninger, A., Colvin, J.S., Vyas, A., Tole, S., Ornitz, D.M. and Bansal, R. (2003) Fibroblast growth factor receptor 3 signaling regulates the onset of oligodendrocyte terminal differentiation. *J. Neurosci.*, **23**, 883–894.
5. Bellus, G.A., Spector, E.B., Speiser, P.W., Weaver, C.A., Garber, A.T., Bryke, C.R., Israel, J., Rosengren, S.S., Webster, M.K., Donoghue, D.J. *et al.* (2000) Distinct missense mutations of the FGFR3 lys650 codon modulate receptor kinase activation and the severity of the skeletal dysplasia phenotype. *Am. J. Hum. Genet.*, **67**, 1411–1421.
6. Iwata, T., Li, C.L., Deng, C.X. and Francomano, C.A. (2001) Highly activated Fgfr3 with the K644M mutation causes prolonged survival in severe dwarf mice. *Hum. Mol. Genet.*, **10**, 1255–1264.
7. Martinez-Frias, M.L., Ramos-Arroyo, M.A. and Salvador, J. (1988) Thanatophoric dysplasia: an autosomal dominant condition? *Am. J. Med. Genet.*, **31**, 815–820.
8. Shigematsu, H., Takashima, S., Otani, K. and Ieshima, A. (1985) Neuropathological and Golgi study on a case of thanatophotoric dysplasia. *Brain Dev.*, **7**, 628–632.
9. Yamaguchi, K. and Honma, K. (2001) Autopsy case of thanatophoric dysplasia: observations on the serial sections of the brain. *Neuropathology*, **21**, 222–228.
10. Langer, L.O., Jr, Yang, S.S., Hall, J.G., Sommer, A., Kottamasu, S.R., Golabi, M. and Krassikoff, N. (1987) Thanatophoric dysplasia and cloverleaf skull. *Am. J. Med. Genet. Suppl.*, **3**, 167–179.
11. Wongmongkolrit, T., Bush, M. and Roessmann, U. (1983) Neuropathological findings in thanatophoric dysplasia. *Arch. Pathol. Lab. Med.*, **107**, 132–135.
12. Coulter, C.L., Leech, R.W., Brumback, R.A. and Schaefer, G.B. (1991) Cerebral abnormalities in thanatophoric dysplasia. *Childs. Nerv. Syst.*, **7**, 21–26.
13. Hori, A., Friede, R.L. and Fischer, G. (1983) Ventricular diverticula with localized dysgenesis of the temporal lobe in cloverleaf skull anomaly. *Acta. Neuropathol. (Berl.)*, **60**, 132–136.
14. Ho, K.L., Chang, C.H., Yang, S.S. and Chason, J.L. (1984) Neuropathologic findings in thanatophoric dysplasia. *Acta. Neuropathol. (Berl.)*, **63**, 218–228.
15. Tavormina, P.L., Shiang, R., Thompson, L.M., Zhu, Y.Z., Wilkin, D.J., Lachman, R.S., Wilcox, W.R., Rimoin, D.L., Cohn, D.H. and Wasmuth, J.J. (1995) Thanatophoric dysplasia (types I and II) caused by distinct mutations in fibroblast growth factor receptor 3. *Nat. Genet.*, **9**, 321–328.
16. Iwata, T., Chen, L., Li, C., Ovchinnikov, D.A., Behringer, R.R., Francomano, C.A. and Deng, C.X. (2000) A neonatal lethal mutation in FGFR3 uncouples proliferation and differentiation of growth plate chondrocytes in embryos. *Hum. Mol. Genet.*, **9**, 1603–1613.
17. Williams, R.W. (2000) *Mapping Genes that Modulate Mouse Brain Development: a Quantitative Genetic Approach*. Springer, New York.
18. Metzger, D. and Chambon, P. (2001) Site- and time-specific gene targeting in the mouse. *Methods*, **24**, 71–80.
19. Kalache, K.D., Lehmann, K., Chaoui, R., Kivelitz, D.E., Mundlos, S. and Bollmann, R. (2002) Prenatal diagnosis of partial agenesis of the corpus callosum in a fetus with thanatophoric dysplasia type 2. *Prenat. Diagn.*, **22**, 404–407.
20. Green, P.J., Walsh, F.S. and Doherty, P. (1996) Promiscuity of fibroblast growth factor receptors. *Bioessays*, **18**, 639–646.
21. Peters, K., Ornitz, D., Werner, S. and Williams, L. (1993) Unique expression pattern of the FGF receptor 3 gene during mouse organogenesis. *Dev. Biol.*, **155**, 423–430.
22. Reid, S. and Ferretti, P. (2003) Differential expression of fibroblast growth factor receptors in the developing murine choroid plexus. *Dev. Brain Res.*, **141**, 15–24.
23. Bansal, R., Kumar, M., Murray, K., Morrison, R.S. and Pfeiffer, S.E. (1996) Regulation of FGF receptors in the oligodendrocyte lineage. *Mol. Cell. Neurosci.*, **7**, 263–275.
24. Kalyani, A.J., Mujtaba, T. and Rao, M.S. (1999) Expression of EGF receptor and FGF receptor isoforms during neuroepithelial stem cell differentiation. *J. Neurobiol.*, **38**, 207–224.
25. Liu, Y., Wu, Y., Lee, J.C., Xue, H., Pevny, L.H., Kaprielian, Z. and Rao, M.S. (2002) Oligodendrocyte and astrocyte development in rodents: an in situ and immunohistological analysis during embryonic development. *Glia*, **40**, 25–43.